International Symposium
On Turbulence and Shear Flow
Phenomena (TSFP-8)
August 28 - 30, 2013 Poitiers, France

THREE-DIMENSIONAL SPECTRAL ANALYSIS OF AN AXISYMMETRIC SEPARATING/REATTACHING FLOW

R. Pain, P. E. Weiss and S. Deck
Department of Applied Aeronautics
ONERA - The French Aerospace Lab
F-92190, Meudon, France
romain.pain@onera.fr

ABSTRACT

The numerical investigation of a high Reynolds number compressible separating-reattaching flow around a simplified space launcher afterbody is carried out using Zonal Detached Eddy Simulation (ZDES). The geometry consists of a cylinder extended by another cylinder of smaller diameter. Spectral analysis of the three-dimensional unsteady pressure field is carried out by means of a discrete Fourier approach as well as a dynamic mode investigation. First, the visualisation of the Power Spectral Density (PSD) around the geometry evidences that high fluctuating energy areas are located on the second half of the emerging cylinder on the skin of the same geometry. It is revealed that such high PSD areas are associated with low frequencies which is often the case for separated flows. The analysis of the dynamic mode associated with the vortex shedding Strouhal number $St_D = \frac{fD}{U_\infty} = 0.18$ exhibits a large scale double-helical organisation which is consistent with results from other investigations in the literature using alternative post-processing tools at lower Reynolds numbers.

INTRODUCTION

Within the atmospheric flight of a space launcher, the flow around the propulsion stage is ruled by the complex dynamics of vortical structures. The drastic pressure fluctuations due to a highly turbulent flow separation expose the nozzle to unsteady and potentially intense loads. The so-called *Buffeting* mode, identified as the azimuthal mode $m = 1$, is likely to trigger loads which can disturb the stability of the launcher and cause severe damages to the payload. In the literature, various geometries were used in order to investigate flow-induced forces such as for axisymmetric bluff bodies as in Eldred (1961), Deprés *et al.* (2004), Deck & Thorigny (2007), and Weiss *et al.* (2009) or suddenly expanded flows as in Gagnon *et al.* (1993). In the bluff body case, it was revealed that mechanical efforts are mainly induced by the oscillatory dynamics of the recirculation bubble. With the intention to evidence such dynamics and investigate their natural frequencies on an axisymmetric backward facing step, Deck & Thorigny (2007) showed by means of two-point correlation analysis on a crown of sensors that the azimuthal mode $m = 1$ contributes to more than 50% of the total energy at a dimensionless frequency $\frac{fD}{U_\infty} = 0.2$ associated to the vortex shedding. Using a local stability analysis, Weiss *et al.* (2009) have recently confirmed that the $m = 1$ antisymmetric mode is dominated by a helical organisation (as suggested by Fuchs *et al.* (1979)) associated to an absolute instability. However, the unsteady spatial organisation associated with the characteristic frequencies of the flow is still not fully understood. The aim of this paper is twofold. First, the Power Spectral Density analysis is extended from 2D (as in Weiss & Deck (2011)) to 3D dataset in order to track the flow dynamics responsible for the PSD distribution at the wall which has been previously derived. Finally, the Fourier modal analysis is applied to the 3D database in order to unveil the spatial organisation associated with a given frequency.

The geometrical setup as well as the numerical strategy are described in the first section. Then it is provided a brief description of the unsteady flow field deriving from the numerical simulation prior to the presentation of the Power Spectral Density and dynamic mode analyses around the emerging cylinder. The main conclusions are given in the last section.

TEST CASE AND NUMERICAL SETUP

The geometry studied is an axisymmetric backward facing step presented in figure 1. The characteristic aspect ratios are chosen to fit with existing experimental models at ONERA, as that of Deprés *et al.* (2004) or Meliga & Reijasse (2007), based on a simplified launcher geometry.

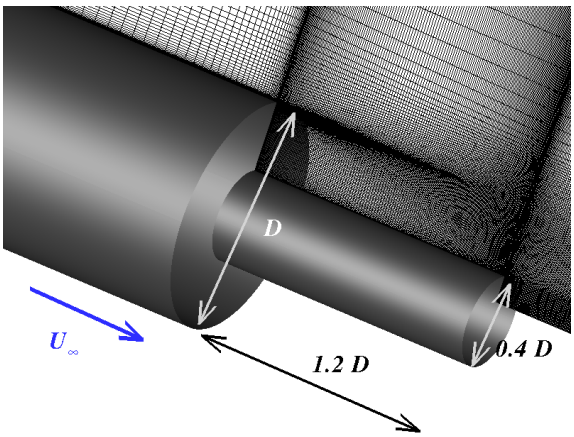

Figure 1. Characteristic dimensions and main direction of the flow.

The computational grid contains 12×10^6 points distributed on a structured multiblock mesh and have 240 points in the azimuthal direction (i.e. 1.5° per plan). The grid is locally refined in the separation area, in particular close to the separation edge (figure 1) in order to model the early stage of the mixing layer instability. In addition, the vorticity thickness of the mixing layer is discretised over 15 points as recommended by Simon *et al.* (2007). This resolution increases in the streamwise direction as the shear layer develops and as the vorticity thickness grows. The Reynolds number based on the greatest diameter D is $Re_D = 1.2 \times 10^6$ and the free stream Mach number is $M_\infty = 0.702$. The initial external boundary layer thickness ratio δ/D is equal to 0.2 at the separation edge of the body with diameter D.

The numerical simulation was performed using the Zonal Detached Eddy Simulation approach developped by Deck (2005, 2012) and implemented in the finite volume solver FLU3M (Guillen & Dormieux (1989)). The FLU3M code developed by ONERA has been assessed on various applications and in particular on launcher geometries (Deck & Thorigny (2007), Simon *et al.* (2007), Weiss *et al.* (2009), Weiss & Deck (2011)). In these last references, the numerical results are thoroughly compared with the available experimental data and second-order analysis. The ZDES zonal hybrid RANS/LES method is well-fitted for massively separated flows, due to the quick switch from RANS to LES near the separation point which avoids delays in the development of the instabilities. The strategy of this method is to select the flow areas (see Deck (2012)) to be computed with RANS or LES according to the problem of interest as illustrated in figure 2.

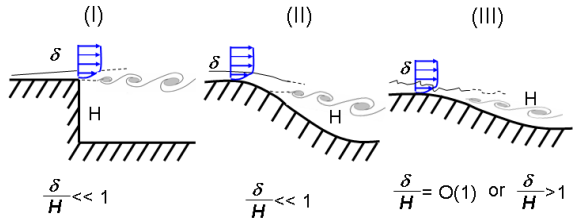

Figure 2. Classification of typical flow problems in the frame of ZDES. I: separation fixed by the geometry, II: separation induced by a pressure gradient on a curved surface, III: separation strongly influenced by the dynamics of the incoming boundary layer. (from Deck (2012)).

In the present case, ZDES is applied in its first mode since the flow separation is triggered by a sharp geometric discontinuity. The time integration of the discretised Navier-Stokes equations is performed by means of the second order accurate backward Gear scheme and the spatial scheme is a modified AUSM+ Liou (1996). The physical time step is $\Delta t = 2 \times 10^{-6}$ s which corresponds to $\Delta \tilde{t} = \Delta t U_\infty / D = 4.7 \times 10^{-3}$. Finally, four inner Newton-Raphson sub-iterations per time step enabled a residual decay of at least one order of magnitude during the convergence process.

RESULTS AND DISCUSSION

First, the instantaneous data of the ZDES simulation are represented in figure 3 with a visualisation of the coherent structures around the afterbody by means of isosurfaces of the normalised Q-criterion: $QU_\infty^2/D^2 = 50$ (with $Q = -\frac{1}{2}\frac{\partial u_i}{\partial x_j}\frac{\partial u_j}{\partial x_i}$). Contours of numerical Schlieren are plotted on the skin of the emerging cylinder and in a streamwise cut-off plane. Very close to the edge of the step, one can clearly identify a sequence of toroïdal structures denoting the roll-up of the shear layer (known as the Kelvin-Helmholtz instability). As analysed by Deck & Thorigny (2007) and Weiss *et al.* (2009), these coherent structures merge together as they are being convected downstream (pairing phenomenon), grow in size, then distort into 3D structures with a hairpin shape near the solid reattachment and finally adopt a fully three dimensional organisation in the wake region.

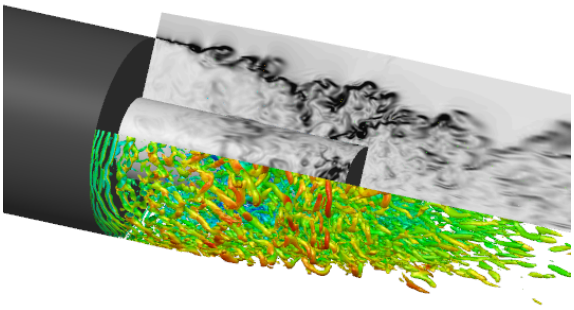

Figure 3. Isosurfaces of the normalised Q-criterion ($QU_\infty^2/D^2 = 50$) coloured by the streamwise velocity with contours of numerical Schlieren (grey scale) on the skin of the emerging cylinder and in a cut-off plane through the main flow direction.

Spectral analysis of the fluctuating pressure field

A Discrete Fourier Transform approach was used in order to compute the Power Spectral Density spectrum for the fluctuating pressure field ($p'(t) = p(t) - \overline{p}$). The 3D spectral analysis consisted in computing the PSD spectrum noted $G(f)$ at each point in the computational domain shown with red bounds in figure 4 *(left)*. The input 3D dataset for the PSD analysis is acquired over a total acquisition period $T_{acq} = 0.2$ s with a sampling rate $f_s = \frac{1}{\Delta t_s} = 100$ kHz (where Δt_s is the time interval between each sample) in order to avoid any aliasing issues. The total acquisition volume consists of 4.5×10^6 points corresponding to 2 T-bytes in memory storage. The Power Spectral Density describes how the levels of fluctuations are distributed in the frequency space and is defined as follows:

$$\sigma^2 = \int_0^\infty G(f)\mathrm{d}f = \int_0^\infty fG(f)\mathrm{d}\left[\log(f)\right] \qquad (1)$$

where σ is the standard deviation of the input signal. For convenience, $G(f)$ spectra are plotted as a function of the Strouhal number $St_D = fD/U_\infty$ which is the normalised frequency.

Figure 4 presents the main steps of the 3D PSD analysis in order to select only the most energetic frequencies. First, the process consists in extracting the maximum value

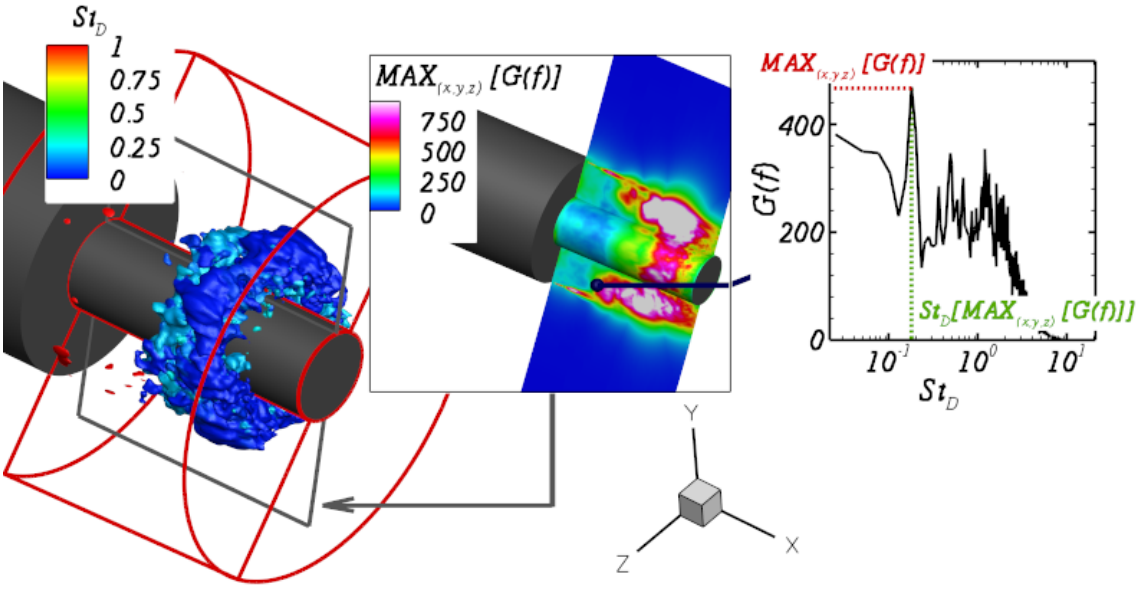

Figure 4. Power Spectral Density (PSD) analysis.*(left)* Isosurface $max_{(x,y,z)}[G(f)] = 900\ Pa^2.Hz^{-1}$ coloured by the Strouhal number St_D. *(middle)* Contours of the maximum value for $G(f)$ at each point of the streamwise cut-off plane ($max_{(x,y,z)}[G(f)]$). *(right)* PSD spectrum associated with the position located in figure 4 *(middle)*.

of $G(f)$ noted $max_{(x,y,z)}[G(f)]$ and the corresponding value $St_D(max_{(x,y,z)}[G(f)])$ at each point in the domain as illustrated in figure 4 *(right)*. As this process is iterated for every point in the acquisition volume, this leads to the three-dimensional distribution of $max_{(x,y,z)}[G(f)]$ shown in figure 4 *(middle)* in a streamwise cut-off plane. In this figure, it appears that the highest levels of PSD are located in the mixing layer close to the separation edge and on the second half of the recirculation bubble. The wall signature of this large area corresponds to high RMS wall pressure coefficient values as evidenced by Deck & Thorigny (2007) and is likely to be due to the growth of the coherent structures from the shear layer as the vortices are pairing. This is consistent with the results from Hudy *et al.* (2003) who suggested that such an increasing fluctuating rate close to the reattachment point is due to the impingement of the coherent structures from the mixing layer on the wall.

Finally, the isosurface $max_{(x,y,z)}[G(f)] = 900\ Pa^2.Hz^{-1}$ is plotted in figure 4 *(left)*. This isosurface corresponds to the area where approximately 60% of the global maximum value for $max_{(x,y,z)}[G(f)]$ in the entire acquisition volume is located. The isosurface is coloured by the Strouhal number associated with the PSD peak $St_D(max_{(x,y,z)}[G(f)])$. It appears that such an energetic area is associated with Strouhal numbers $St_D \leq 0.25$ and is located mainly on the second half of the domain, forming a crown around the emerging cylinder. The size of this crown is of the order of one step height which highlights that most of the energy is contained in the recirculation area.

In addition, the contours of $St_D(max_{(x,y,z)}[G(f)])$, the most energetic normalised frequencies are presented in figure 5 in a streamwise cut-off plane. Four main flow dynamics corresponding to four different normalised frequencies can be identified. Dynamics in area III corresponds to the vortex shedding ($St_D \sim 0.2$) and is located in the interval $0.4 \leq x/D \leq 0.75$. This corroborates the results of Weiss *et al.* (2009) who derived the existence of an absolutely unstable area associated with the vortex shedding in the same space interval. On each side of zone III are located two zones with $St_D \sim 0.03$ which is associated with the flapping motion of the mixing layer and the streamwise oscillations of the instantaneous reattachment point as in Kiya & Sasaki (1983). Finally, area II is associated with the Kelvin-Helmholtz dynamics occurring in the shear layer, and area IV corresponds to the wake dynamics by the end of the geometry.

Modal analysis

The aim is now to investigate the spatial organisation associated with the Strouhal numbers identified above with the view to provide a deeper insight into the flow mechanisms and in particular those responsible for the unsteady side-loads. In practice, such an analysis is usually fulfilled by decomposing the flow structures into modes. To this end, the Fourier mode decomposition method is used in this paper since each Fourier mode is characterised by its own frequency and energy level. A comparison with the recent Dynamic Mode Decomposition method (Rowley *et al.* (2009),Schmid (2010)) is briefly performed, with the view to cross-check the first analysis.

Fourier modes The temporal Discrete Fourier Transform provides Fourier modes defined on a given frequency range. Such Fourier modes, denoted $X(f)$ here, are computed by means of a Welch periodogram. It consists in dividing the raw input signal into overlapping blocks of equal frequency length and resolution. The hereby spectral investigations are carried out on a frequency window ranging from 5 Hz ($St_D = 2 \times 10^{-3}$) to 100 kHz ($St_D = 42.2$) by steps of $\Delta f = 60$ Hz ($St_D \sim 2.5 \times 10^{-2}$). The total CPU time elapsed was approximately 20 h for the processing of the $4,600,000$ pressure signals discretised in $N = 20,000$ snapshots with $T = 200$ ms. While the previous section focused on the Power Spectral Density $G_{p'}(f)$ of each Fourier mode (i.e. the square modulus of $X(f)$ over the integration period for each frequency band Δf), this paragraph concentrates on the complex Fourier mode at each point in the

computational volume (shown in figure 4). The complex Fourier modes associated with the vortex-shedding ($St_D = 0.18$) was extracted as it has been identified as the most contributing dynamics in the unsteady side-loads (Deprés *et al.* (2004) and Deck & Thorigny (2007)). In addition, $St_D = 0.6$ is investigated as it constitutes an energetic frequency by the end of the geometry. The imaginary part of each of those Fourier modes is depicted in figures 6 and 7 respectively.

Contours of $\Im\left[X_{St_D=0.18}(f)\right]$ (figure 6) clearly exhibit a sequence of two diametrically opposed positive and negative large scale regions. Such an antiphase behaviour is consistent with the experimental results from Deprés *et al.* (2004) and the numerical investigations of Deck & Thorigny (2007) on the same geometry with a jet. Both of these authors evidenced that the azimuthal mode $m = 1$ strongly dominates the vortex shedding frequency.

The hereby visualisation of the three-dimensional Fourier mode associated to $St_D = 0.18$ therefore enables to evidence the spatial organisation of the fluctuating pressure field which is mainly responsible for the aerodynamic unsteady side-loads. The phase shift of the positive and negative pressure areas indeed induces an imbalance of the force acting on the wall. Besides, the wave length in the streamwise direction approximately amounts for $2L = 2.4D$ (L is the length of the cylinder with diameter $d = 0.4D$ see figure 1). This is in agreement with the maximum absolute wavelength $\lambda_0 = 2.6$ derived by Weiss *et al.* (2009) by means of

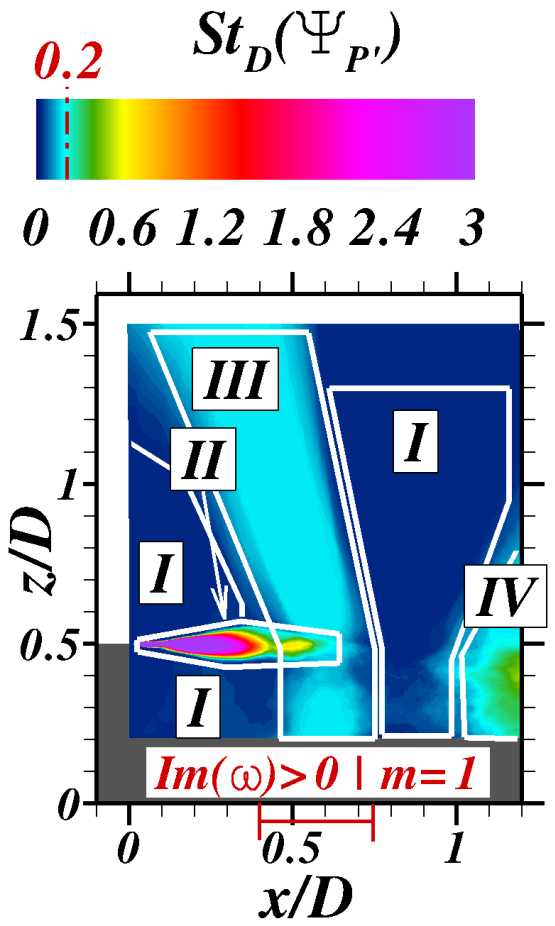

Figure 5. Spectral map of the most energetic frequencies $St_D(max_{(x,y,z)}\left[G(f)\right])$.

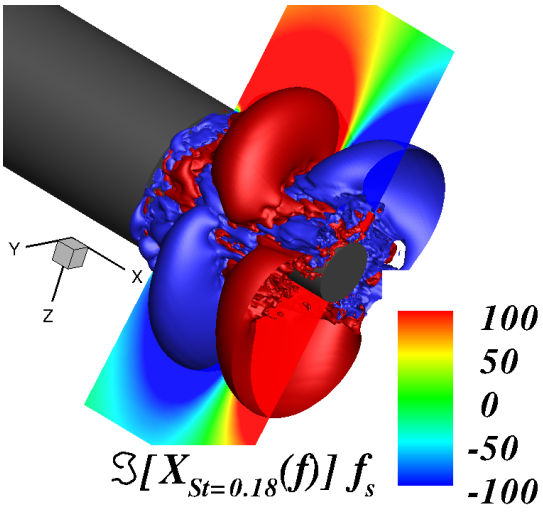

Figure 6. Contours of $\Im\left(X\left(f\right)\right) \times f_s$ in Pa and isosurfaces of $\Im\left(X\left(f\right)\right) \times f_s = \pm 200$ Pa of the Fourier mode associated with $St_D = 0.18$.

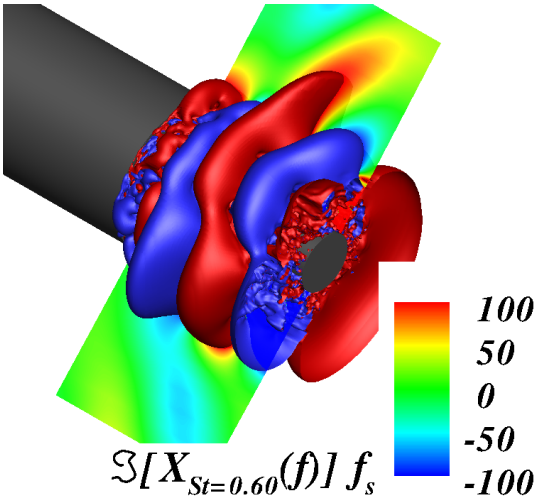

Figure 7. Contours of $\Im\left(X\left(f\right)\right) \times f_s$ in Pa and isosurfaces of $\Im\left(X\left(f\right)\right) \times f_s = \pm 200$ Pa of the Fourier mode associated with $St_D = 0.60$.

a local linear stability analysis.

The spatial distribution of the Fourier mode related to $St_D = 0.6$ is similar to that of $St_D = 0.18$ with a shorter streamwise wave length ($\lambda_x \simeq 0.7D$).

Dynamic modes The recent Dynamic Mode Decomposition derived by Rowley *et al.* (2009) and Schmid (2010) has been used in this section with the view to support the results of the previous section. This method relies on the spectral analysis of a linear operator called the Koopman operator (Rowley *et al.* (2009)) and each dynamic mode is characterised by its own frequency. Chen *et al.* (2012) have mathematically shown that DMD on mean-subtracted input data is equivalent to the temporal Discrete Fourier Transform. As such, this method is a well-adapted tool to compare with the Fourier results.

In order to reduce the CPU costs involved for the application of such a post-processing, a subset of the total numer-

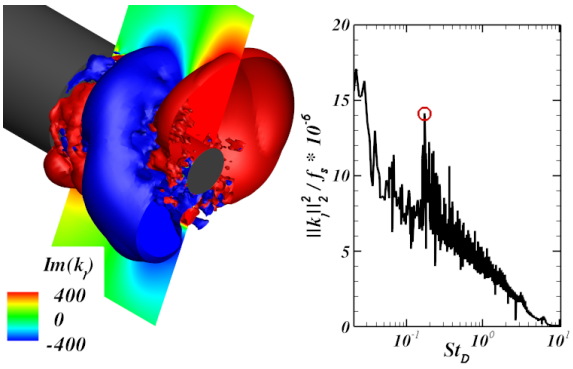

Figure 8. *(left)* Isosurfaces of the imaginary part of the dynamic mode associated with $St_D = 0.18$ ($\mathbf{k_j}$: $\Im(\mathbf{k_j}) =$ 50 Pa (*red*) and $\Im(\mathbf{k_j}) = -50$ Pa (*blue*)) with contours of $\Im(\mathbf{k_j})$ in a streamwise cut-off plane. *(right)* Dynamic mode analysis spectrum: normalised norm of the dynamic modes as a function of the Strouhal number. The dynamic mode represented on the left is circled in red.

ical data is considered consisting of $N = 10,000$ snapshots with a time interval of $4.7 \cdot 10^{-2} D/U_\infty$ providing maximum and minimum resolvable Strouhal numbers of respectively 10.55 and 0.0021 based on the Nyquist-Shannon criteria. Besides, the dynamic modes were computed on a coarser grid consisting of $35 \times 23 \times 121$ points. This coarser mesh was derived from the initial one using space modulos in all three directions. The following scalar product, derived from Aubard *et al.* (2011), is used to project the dynamics on a lower-dimensional space:

$$\int\int\int \left[\frac{\rho u_i'^2}{2} + \frac{p'^2}{2\gamma \bar{P}} \right] dxdydz \qquad (2)$$

The computation of the Koopman modes for the entire volume shown in figure 4 is performed by means of the DMD algorithm described by Schmid (2010). The approximated CPU time including reading the snpashot files, the computation of the Companion matrix (Rowley *et al.* (2009),Schmid (2010)) and the eigenproblem resolution amounted for 88 hours with an in-house sequential code.

Each of the eigenvalues is associated with one dynamic mode $\mathbf{k_j}$ whose frequency is given by $f_j = \Im\left(\log(\lambda_j)\right)/2\pi\Delta t$, where λ_j is the eigenvalue associated with $\mathbf{k_j}$.

Figure 8 *(right)* depicts the DMD spectrum with the normalised norm of the dynamic modes ($\| \mathbf{k_j} \|_2^2 / f_s$ where f_s is the sampling frequency, $\mathbf{k_j}$ is the dynamic mode number j, and $||\bullet_j||_2^2 = \sqrt{(\bullet_{j,1})^2 + (\bullet_{j,2})^2 + \ldots + (\bullet_{j,m})^2}$ is the L_2-norm) as a function of the Strouhal number St_D.

The spectrum features a sequence of peaks, from low to high frequency ranges, with some of them clearly distinguable by their higher magnitude. Let us focus on $St_D = 0.18$, circled in red in the spectrum, as it appears to be one of the dominant dynamics. In figure 8 *(left)* is presented the shape of the corresponding dynamic mode with the contours of the imaginary part of $\mathbf{k_j}$ in a cut-off plane. According to the isosurfaces $\Im(\mathbf{k_j}) = 200$ Pa and $\Im(\mathbf{k_j}) = -200$ Pa, it is observed that the structures form an anti-clockwise large-scale double helical organisation. Such a spatial organisation seems to be consistent with the results of Monkewitz (1988) who evidenced that the preferred instability mode in the axi-symmetric wake is a spiral at low and moderate Reynolds numbers. This has also been put forward by Sandberg & Fasel (2006) for the supersonic regime by means of local stability calculations.

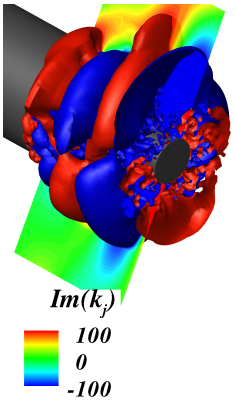

Figure 9. Isosurfaces of the imaginary part of the dynamic mode associated with $St_D = 0.60$ ($\mathbf{k_j} : \Im(\mathbf{k_j}) = 100$ Pa (*red*) and $\Im(\mathbf{k_j}) = -100$ Pa (*blue*)) with contours of $\Im(\mathbf{k_j})$ in a streamwise cut-off plane.

Although the spatial distribution of the $St_D = 0.18$ dynamic mode differ from the corresponding Fourier mode, the characteristic wave length in the streamwise direction fit well with each other. Such a discrepancy with the Fourier approach might be due to either the coarser grid and time resolution or to the difference in the quantity that is decomposed: the Fourier approach deals with the fluctuating pressure field $p'(t)$ while the dynamic mode decomposition deals with the scalar from equation 2.

In opposition, the distribution of the dynamic mode associated with $St_D = 0.6$ is very close to that of the corresponding Fourier mode.

CONCLUSIONS

The Zonal Detached Eddy Simulation (ZDES) of an axisymmetric backward facing step of finite length has been performed at a Reynolds number based on the largest diameter $Re_D = 1.2 \times 10^6$ and a free stream Mach number $M_\infty = 0.7$. A spectral analysis of the three-dimensional data set in the separated zone has been carried out.

First, the analysis of the three-dimensional fluctuating pressure field around the smallest cylinder evidenced an area with high fluctuating energy level located on the second half of the recirculation region. It was evidenced that such an intense pressure fluctuation zone is mainly driven by $St_D \leq 0.25$ dynamics which coincides with the available results from the literature. Several other dynamics, such as $St_D = 0.6$ by the end of the geometry and $St_D \simeq 0.03$ associated with the flapping motion of the mixing layer, were identified as being locally the most energetic frequencies.

Besides, a modal investigation has been performed. The visualisation of the three-dimensional complex Fourier modes highlighted the characteristic spatial organisation associated with $St_D = 0.2$ and $St_D = 0.6$. A pair of two diametrically opposed regions with a phase shift of π was evidenced for the vortex-shedding which is in agreement with

the results of Deprés *et al.* (2004) and Deck & Thorigny (2007) who associated $St_D = 0.2$ with the antisymmetric azimuthal mode $m = 1$. Such a diametrically opposed distribution unveils the behaviour of the $m = 1$ mode which strongly dominates the unsteady side-loads process as emphasized by Weiss *et al.* (2009) for a two-dimensional fluctuating pressure signal.

The use of the dynamic mode decomposition to cross-check the previous modal analysis allowed to confirm the characteristic streamwise wave lengths for $St_D = 0.2$ and $St_D = 0.6$. The spatial distribution of the dynamic mode associated with $St_D = 0.2$ slightly differ from that of the corresponding Fourier mode which might be due to either the difference in space and time resolution between both methods or to the pre-processing process.

The authors thank the Centre National d'Etudes Spatiales (CNES) for financial support. The Ph.D. work of R. Pain is funded by CNES and ONERA.

REFERENCES

Aubard, G., Robinet, J. C. & Gloerfelt, X. 2011 Physical insight into the unsteady shock-wave turbulent boundary layer interaction using large eddy simulation. In *Turbulence and Shear Flow Phenomena*.

Chen, K., Tu, J. H. & Rowley, C. W. 2012 Variants of dynamic mode decomposition: connections between koopman and fourier analyses. *Journal of Nonlinear Science* **22**, 887 – 915.

Deck, S. 2005 Zonal Detached Eddy Simulation of the flow around a high-lift configuration. *AIAA Journal* **43**, 2372 – 2384.

Deck, S. 2012 Recent improvements in the Zonal Detached Eddy Simulation (ZDES) formulation. *Theoretical and Computational Fluid Dynamics* **26**, 523.

Deck, S. & Thorigny, P. 2007 Unsteadiness of an axisymmetric separating-reattaching flow: Numerical investigation. *Physics of Fluids* **19**.

Deprés, D., Reijasse, P. & Dussauge, J. P. 2004 Analysis of unsteadiness in afterbody transonic flows. *AIAA Journal* **12**, 2541–2550.

Eldred, K. M. 1961 Base pressure fluctuations. *The Journal of the Acoustical Society of America* **33**.

Fuchs, H. V., Mercker, E. & Michel, U. 1979 Large-scale coherent structures in the wake of axisymmetric bodies. *Journal of Fluid Mechanics* **93**, 185 – 207.

Gagnon, Y., Giovannini, A. & Hébrard, P. 1993 Numerical simulation and physical analysis of high Reynolds number recirculating flows behind sudden expansions. *Physics of Fluids* **5**, 2377–2389.

Guillen, P. & Dormieux, M. 1989 Design of a 3d multi-domain euler code. In *International Seminar of Supercomputing*.

Hudy, L. M., Naguib, A. M. & Humphreys, W. M. Jr. 2003 Wall-pressure-array measurements beneath a separating/reattaching flow region. *Physics of Fluids* **15**.

Kiya, M. & Sasaki, K. 1983 Structure of a turbulent separation bubble. *Journal of Fluid Mechanics* **137**, 83 – 113.

Liou, M.-S. 1996 A sequel to AUSM: AUSM+. *Journal of Computational Physics* **129**, 364 – 382.

Meliga, P. & Reijasse, P. 2007 Unsteady transonic flow behind an axisymmetric afterbody equipped with two boosters. In *25th AIAA Fluid Dynamics Conference and Exhibit*.

Monkewitz, P. 1988 A note on vortex shedding from axisymmetric bluff bodies. *Journal of Fluid Mechanics* **192**, 561 – 575.

Rowley, C. W., Mezić, I., Bagheri, S., Schlatter, P. & Henningson, D. S. 2009 Spectral analysis of nonlinear flows. *Journal of Fluid Mechanics* **641**, 115–127.

Sandberg, R. D. & Fasel, H. F. 2006 Numerical investigation of transitional supersonic axisymmetric wakes. *Journal of Fluid Mechanics* **563**, 1 – 41.

Schmid, P. J. 2010 Dynamic mode decomposition of numerical and experimental data. *Journal of Fluid Mechanics* **656**, 5–28.

Simon, F., Deck, S., Guillen, P., Sagaut, P. & Merlen, A. 2007 Numerical simulation of the compressible mixing layer past an axisymmetric trailing edge. *Journal of Fluid Mechanics* **591**, 215 – 253.

Weiss, P. E. & Deck, S. 2011 Control of the antisymmetric mode (m=1) for high Reynolds axisymmetric turbulent separating/reattaching flows. *Physics of Fluids* **23**, 095102.

Weiss, P. E., Deck, S., Robinet, J. C. & Sagaut, P. 2009 On the dynamics of axisymmetric turbulent separating/reattaching flows. *Physics of Fluids* **21**, 075103.